Mechanistic insight into the kinetic fragmentation of Norpinonic Acid in the gas phase: An experimental and DFT study

Izabela Kurzydym[1,3], Agata Błaziak[2], Kinga Podgórniak[1,3], Karol Kułacz[1,3], Kacper Błaziak[*,1,3]

[1]Faculty of Chemistry, University of Warsaw, ul. Pasteura 1, 01-224 Warsaw, Poland
5 [2]Institute of Physical Chemistry, Polish Academy of Sciences, Warsaw 01-224, Poland
[3]Biological and Chemical Research Center, University of Warsaw, ul. Żwirki i Wigury 101, 01-224 Warsaw, Poland

Correspondence to: Kacper Błaziak (kblaziak@chem.uw.edu.pl)

Abstract. Norpinonic acid has been known as an important α-pinene atmospheric Secondary Organic Aerosol (SOA) component. It is formed in the reaction of α-pinene, β-pinene or verbenone with atmospheric oxidizing reagents. In the
10 presented study, tandem mass spectrometry techniques were used to determine the exact norpinonic acid fragmentation pathway in the gas phase. The precursor anion – deprotonated norpinonic acid (m/z 169) generated in an electrospray (ESI) source were subjected into the collision cell of the mass spectrometer and fragmented using Energy-Resolved Collision Induced Dissociation (ER-CID) technique. The experimental energy values –of degradation processes were determined via analysis of the breakdown curves.. Quantum chemical calculations of the reaction models were also constructed, including
15 calculation of all transition states. Comparison between the experimental and the theoretical threshold energies calculated at ωB97XD/6-311+G(2d,p) level of theory has shown a good correlation. Two basic pathways of the fragmentation of the parent anion $[M-H]^-$ (m/z 169) were observed. A first, lead to the decarboxylation product (m/z 125) and second to the loss of neutral molecule (C_4H_6O) together with the formation of anion m/z 99. On the other hand, the breakdown of anion m/ z 125 gives a rise of m/ z 69, 57, and 55 ions. To confirm structures formed during ER-CID experiments, the gas-phase proton transfer
20 reactions were examined of all Norpinonic acid anionic fragments with a series of neutral reagents, characterized by Proton Affinity (PA) values. Based on PA differences analysis, the most possible chemical structures were proposed for the observed fragment anions.

1 Introduction

Earth's atmosphere contains a tremendous amount of organic compounds, which differ in fundamental properties such as,
25 volatility, reactivity, hygroscopicity and propensity to form cloud droplets (Hallquist et al., 2009). It is estimated that 10 000 to 100 000 different organic compounds have been measured in the atmosphere (Goldstein, 2007). Primary organic aerosols are emitted to the atmosphere directly from a wide variety of natural and anthropogenic sources (Hallquist et al., 2009). Globally, about 1300 Tg of volatile organic compounds (VOC) are emitted each year to the atmosphere, from biomass burning, combustion of fossil fuels, volcanic eruptions, vegetation processes (Seinfeld and Pandis, 2016; Olsson and Benner, 1999).
30 The chemical reactions of VOCs with different atmospheric oxidizing reagents, such as ozone (O_3), OH radicals and NO_3 radicals result in SOA formation (Gómez-González et al., 2012; George and Abbatt, 2010; Kavouras et al., 1999).

Studies on the chemical composition of SOA have reported the formation of a number of multifunctional products, among which, a large number of compounds containing carboxylic functional groups. Due to their low volatility, mono, di- and tricarboxylic acids have been also suggested as key species in gas-to-particle conversion processes (Claeys et al., 2007; E.

35 Jenkin et al., 2000; Glasius et al., 2000; Christoffersen et al., 1998). Norpinonic acid is considered a semi-volatile organic compound (SVOC) with a vapor pressure of about 1.28×10^{-4} Torr,[cytownie] making it a slightly more significant contributor to the gas-phase air chemical composition than pinic, pinonic, or norpinic acids. Considering this, the potential gas-particle phase transition of Norpinonic acid suggests that it's kinetic transformations in gas phase may play an important role in atmosphere evolution (Ruff, 2018).

40 Field studies have shown that a few organic acids formed during α-pinene oxidation process, such as pinic acid, pinonic acid, norpinic acid, norpinonic acid and their isomers, are prominent components of atmospheric aerosol natural samples (Feltracco et al., 2018; Lignell et al., 2013; Kavouras et al., 1998).

The analytical toolbox available for chemists to study atmospheric organic components has expanded considerably during the past decades (Hallquist et al., 2009). A wide variety of analytical techniques are used to the structural characterization of

45 organic aerosol (OA) products, e.g., gas chromatography/mass spectrometry (GC/MS) (Shao et al., 2022; Tajuelo et al., 2022), liquid chromatography/mass spectrometry (LC/MS) (Resch et al., 2023; Sarang et al., 2023), nuclear magnetic resonance (NMR) (Mcalister et al., 2021; Rodriguez et al., 2022) and Fourier transform infrared (FTIR) spectroscopy (Yu et al., 2021; Zanca et al., 2017; Takahama et al., 2016; Finessi et al., 2012). In particular, liquid chromatography in combination with high-resolution negative ion electrospray ionization mass spectrometry is widely used to identify and quantify the atmospheric

50 aerosol polar and organic compounds (Gómez-González et al., 2012). Identification is mostly based on second-order mass spectra (MS/MS), which together with an elemental composition of target ion signals obtained from high-resolution measurements helps with the structural characterization of the organic compounds (Claeys et al., 2009; Kourtchev et al., 2008; Szmigielski et al., 2007). However, to the proper identification of OA components, mentioned MS/MS measurements should be made very accurately, to have full confidence with the organic compound structural characterization during ambient samples

55 analytical process (Hocart, 2010).

In this publication, we have focused on one of the α-pinene SOA component - Norpinonic acid, which is formed in the reaction of α-pinene with atmospheric oxidizing reagents, such as O_3 or OH radicals (Zhang, 2015; Ma et al., 2008; Ma et al., 2007; Winterhalter et al., 2003; Peeters et al., 2001). Norpinonic acid is considerably significant which is about $0.2 – 1.1$ ng·m^{-3} (Li et al., 2013). It is known, that the majority of the chemical process in the atmosphere are induced by the radical species both

60 in the night and day times. However, it is also proposed that some of the chemical transformations in the atmosphere may proceeds *via* other chemical routes that do not require the presence of radicals, which might go through anionic or cationic pathways e.g. the ion cluster formation or deprotonation of acidic structures by basic inorganic agents (Jarrold, 2023; Richards et al., 2020; Hirsikko et al., 2011; Blanco-Heras et al., 2008; Krivácsy et al., 1997; Mccrumb and Arnold, 1981). Nevertheless, there are no models proposing intra or bimolecular reaction paths, e.g. the kinetic, or thermodynamic energy-induced

65 degradation process that can break SOA or other organic and inorganic components into fragments within ionic chemical

transformations. Organic acids containing one or more carboxylic groups are significant contributors to the total SOA mass and the Norpinonic acid is chosen as an prominent example to rationalize its fragmentation process.

Herein, we studied the Norpinonic acid anionic fragmentation pathway in the gas phase, together with identification of the exact ion fragment structures based on the second-order mass spectrum (MS/MS) recorded during energy resolved collision-induced dissociation mass spectrometry experiments (ER-CID). Detailed analysis of recorded breakdown curves has been provided, which have led to the experimental energy values required gas-phase degradation processes. In addition, structural analysis have been made through the bimolecular reactions of Norpinonic acid anion and it's anionic fragments with a series of neutral reagents (CH_3SCN, CH_3SSCH_3, $CHCl_3$, $CHBr_3$, CH_2Cl_2, CH_3NO_2) to investigate the difference in Proton Affinity (PA) values based on observation of the proton-transfer reaction. Quantum chemical calculations of the reaction models for all observed fragmentation processes were also conducted, including determination of all transition states presented in the reaction mechanism. Improved knowledge of the structures formed during ER-CID-MS experiments leads to a better understanding of potential atmospheric reaction pathways. (Nozière et al., 2015).

2 Experimental section

2.1 General Materials and Methods

C*is*-norpinonic acid was synthesized in the Laboratory of the Environmental Chemistry in the Institute of Physical Chemistry PAS using an optimized synthetic procedure based on previously reported method by Moglioni et al. (Moglioni et al., 2000). A detailed synthetic procedure for the preparation and purification of the norpinonic acid along with the IR, ESI-HR-MS, ^1H and ^{13}C NMR analytical spectra of the final product are provided in Supporting Information (section: 1. Synthesis of investigated compound).

2.2 Mass spectrometry experiments

All experiments were performed using a modified Micromass/Waters Q-ToF 2 spectrometer (Blaziak et al., 2018; Błaziak et al., 2017; Miller et al., 2014) equipped with electrospray (ESI) ion source operated in the negative ion mode. The norpinonic acid anion (*m/z* 169) (International Union Of and Applied) was generated by introducing to the ESI source an aqueous – methanolic (2:1) solution of 1 mM Norpinonic acid using a syringe pump at a flow rate of 0.2 ml/min. The main fragmentation product ions investigated in this work were formed in two ways: upon collision activation in the collision cell by varying the collision kinetic ion energy and in the ion source by varying the capillary and cone voltages accelerating the in-source bond breaking process. For the ER-CID experiments argon (Ar) was used as collision gas, while for the bimolecular gas phase reactions different reagent vapors were introduced to the collision cell using an in-house gas inlet system (Blaziak et al., 2018; Błaziak et al., 2017; Miller et al., 2014). The bimolecular reactions together with proton affinity analyses were carried out to identify the isomeric and conformational diversity of the Norpinonic acid anionic fragments formed both in the collision cell and the ion source of the mass spectrometer. Volatile reagents introduced to the collision cell and used for the bimolecular

reactions as neutral reagents were as follows: methyl thiocyanate, dimethyl disulfide, chloroform, bromoform, dichloromethane and nitromethane. In the present study a full series of the breakdown curves were recorded to determine the onset/threshold energies of the Norpinonic acid fragmentation reactions. Collision spectra were recorded by varying the collision energy in incremental steps with an energy resolution of 8–25 eV in the lab frame and 5-10 minutes of collection time at each step. To enable the comparison of the observed process, a linear fit of the approximately linearly rising section of the breakdown curve was performed for each dataset. The onset energy has been defined at each gas pressure by calculation of the energy (X value) at zero intensity (Y = 0). Additionally, to compare the experimental and theoretical energy landscapes, the gas pressure linear extrapolation has been also performed. The onset energies defined at five different gas pressures were similarly linearly extrapolated to the zero pressure point, giving the final threshold energies reported in this work.

2.3 Quantum chemical calculation

All calculations were performed with Gaussian 09 suite of programs (M. J. Frisch, 2009). The Cartesian coordinates of the initial geometries were created using the GaussView 5.0 program (Dennington R., 2009). The geometries of the reactants, products, intermediates and transition states were optimized using CAM-B3LYP, PBE1PBE and ωB97XD functionals with the same 6-311+G(2d,p) basis set. More description about program and funcionals see SI (section 4). No symmetry restrictions were used during the calculation. Harmonic frequencies were used to identify the ground state structures with all real frequencies and transition states (TS) with only one imaginary frequency. The IRC computations were also performed to ensure that each TS structure corresponds to the desired products and substrates. Zero-point energy (ZPE) corrections were included in energy calculations. A schematic representation of the strategy used to determine the functional that gives the results that most closely approximate the experimental data presented in Figure S62 in SI.

3 Results and discussion

3.1 Fragmentation pathway of Norpinonic acid an anion

Introducing a methanolic-aqueous solution of the norpinonic acid to the electrospray ion source of the mass spectrometer gives a rise to deprotonated anion corresponding to $C_9H_{13}O_3^-$ (m/z 169) in the negative ion mode. Subjecting these ions to collisional activation leads to the formation of fragment ions, corresponding to $C_8H_{13}O^-$ (m/z 125), $C_5H_7O_2^-$ (m/z 99), $C_3H_5O^-$ (m/z 57), $C_4H_5O^-$ (m/z 69), $C_4H_7^-$ (m/z 55) and C_2HO^- (m/z 41) anions. Representative ER-CID mass spectra of $C_9H_{13}O_3^-$ (m/z 169) as well as for fragment ions (m/z 125 and m/z 99) taken at the center-of-mass collision energy (ECM) = 3.8 eV, 4.1 eV and 4.3 eV (CM), respectively, with argon collision gas at nominal pressures of 3.54 ×10⁻⁴ mBar are shown in Fig. 1.
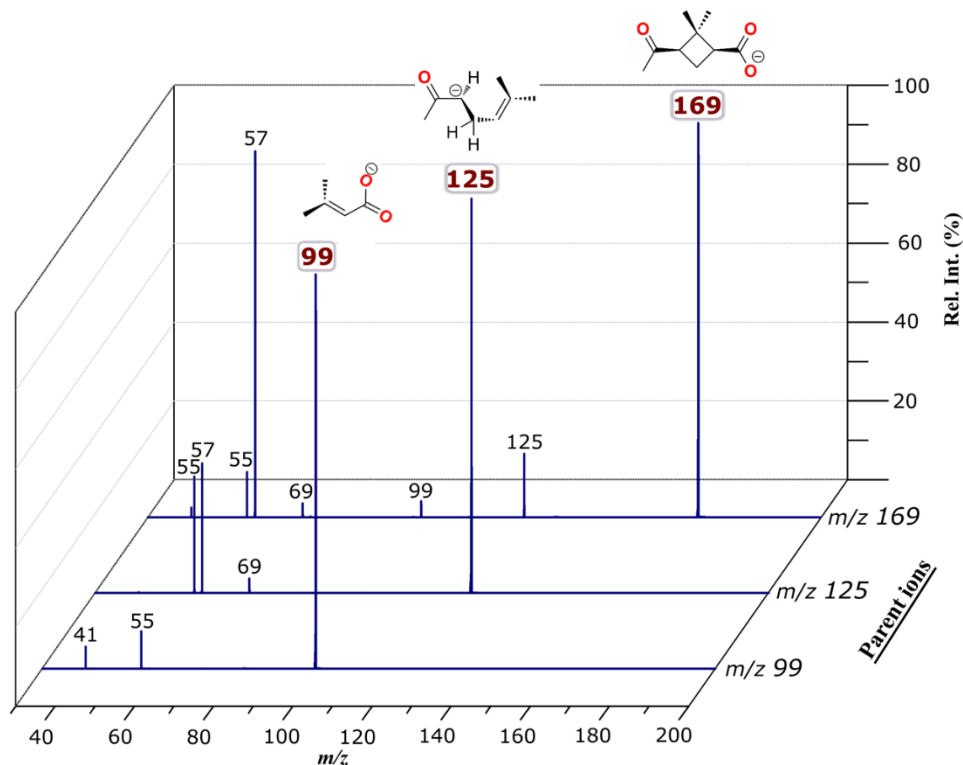
Figure 1. Fragment ion mass spectra of m/z 169, m/z 125 and m/z 99 recorded with a ToF voltage of 3kV, taken at a collision energy of 3.8 eV, 4.1 eV and 4.3 eV (ECM), respectively with argon collision gas at nominal pressures of 3.54 × 10⁻⁴ mBar.

Additionally, to analyze the energetic requirements for each observed fragmentation pathway, the full set of breakdown curves for all of the ions have been recorded, by varying stepwise the kinetic collision energy in five different collision gas pressures. The threshold energies were estimated by employing a simple extrapolation procedure, which in details has been described in Supplementary Information (SI, Figure S8-S11, S13-16, S21-S24, S26-S29, S31-S34, S39-S42 and S44-S47). Figure 2 shows the representative breakdown diagrams of m/z 169, m/z 125 and m/z 99 recorded with Ar collision gas at a nominal pressure of 1.06×10^{-4} mbar, 1.08×10^{-4} mbar, 1.06×10^{-4} mbar, respectively. For other spectra, as well as for additional breakdown curves please consult the SI (Figure S1-S6, S17-S19 and S35-S37).
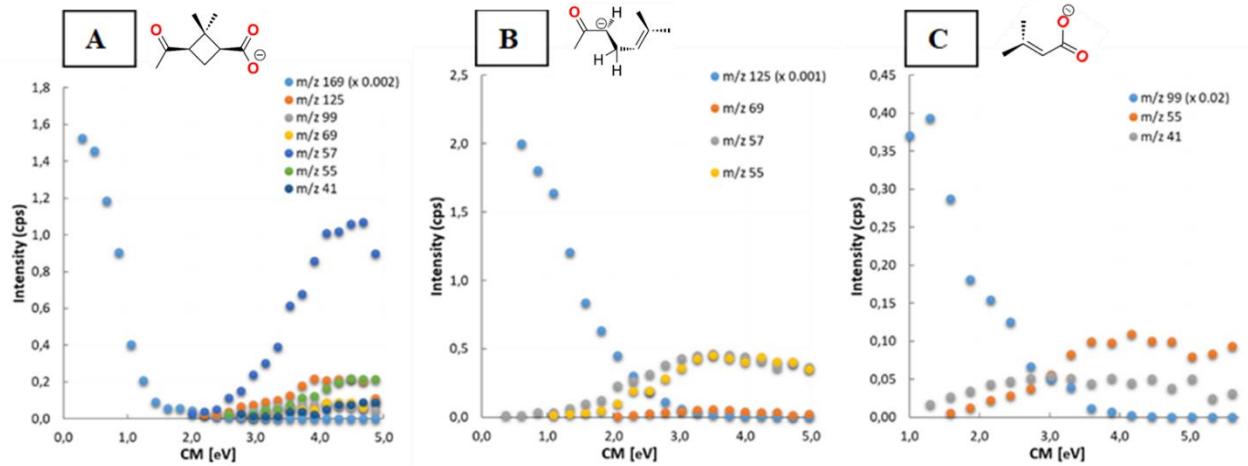
135

Figure 2. Breakdown curves from the CID experiments on m/z 169 (A), m/z 125 (B) and m/z 99 (C) – with the ion intensity for the individual ions as a function of ECM. Please note the different scales of the ordinates. The data were recorded with Ar collision gas at a nominal pressure of 1.06×10^{-4} mbar, 1.08×10^{-4} mbar, 1.06×10^{-4} mbar, respectively.

The experimentally measured reaction energies and the general fragmentation network of the main m/z 169 Norpinonic acid
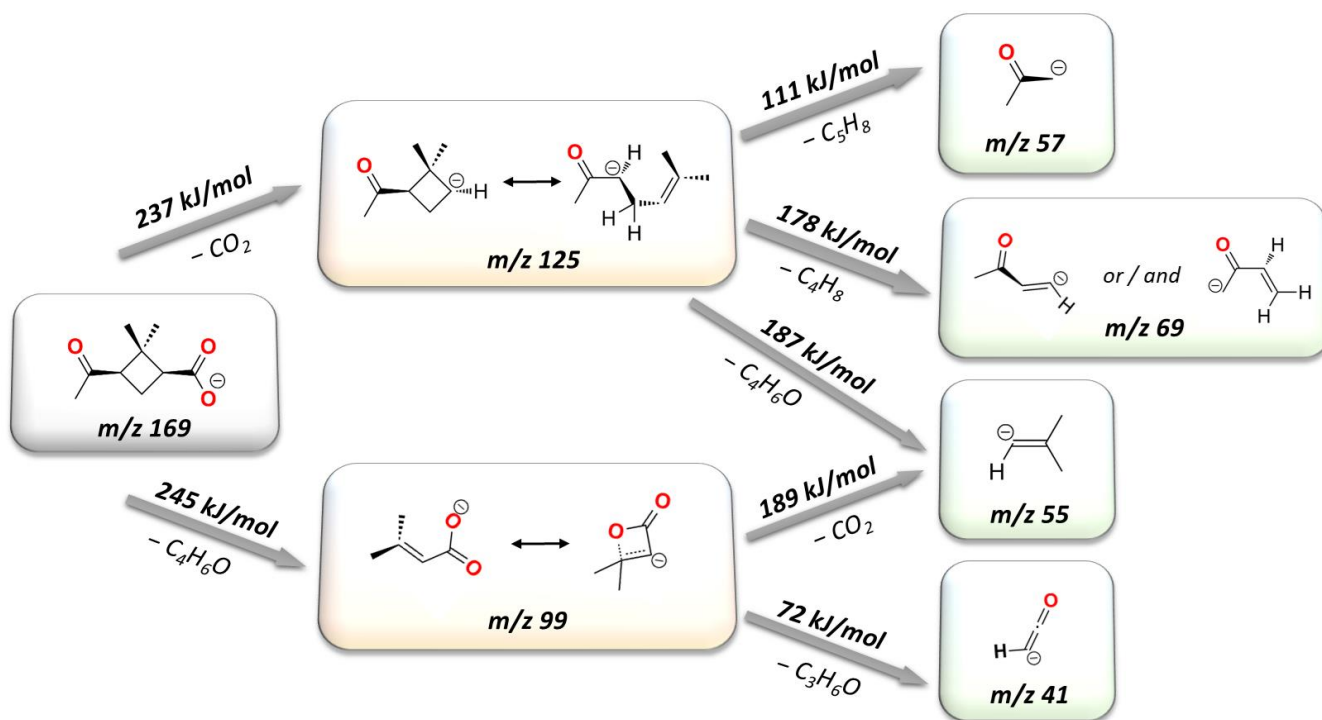
140   anion has been shown in Fig. 3.

Figure 3. The fragmentation network for deprotonated norpinonic acid (m/z 169). Please note that above the gray arrows the experimental threshold energies (kJ/mol) for each fragmentation reaction are shown. Below the arrow is the formula of the neutral particle being dropped off.

It was found that the parent anion $C_9H_{13}O_3^-$ (m/z 169) undergoes two main fragmentation pathways. The first is expressed by the loss of neutral fragment C_4H_6O (mass 70), resulting in formation of $C_5H_7O_2^-$ (m/z 99) anion with an experimentally established appearance energy of 245 ($\pm$ 73) kJ/mol. The second, a decarboxylation reaction leading to $C_8H_{13}O^-$ (m/z 125), with onset energy at 237 ($\pm$ 70) kJ/mol. In order to establish the detailed fragmentation network of the main anion, separate ER-CID experiments were performed for each smaller anionic fragments that were observed on main product-ion spectra. Consequently, on the ER-CID mass spectrum of m/z 99, two secondary fragmentation products have been observed. The formation of C_2HO^- (m/z 41) followed by the loss of the neutral molecules C_3H_6O (see Fig. 5 below), with estimated fragmentation energy at 72 ($\pm$ 22) kJ/mol. Anion $C_5H_7O_2^-$ (m/z 99) was also prone to loss carbon dioxide molecule (see Fig. 5 below), which leads to the formation of $C_4H_7^-$ (m/z 55) anion, at the energy of 189 ($\pm$ 57) kJ/mol. The separate ER-CID experiment for m/z 125 anion has shown, that in-cell activation leads to three different fragmentation pathways. In the first route, m/z 69 anion is formed by the loss of the neutral molecule C_4H_8 (mass 56; see Fig. 4 below), with an experimentally established appearance energy of 178 ($\pm$ 53) kJ/mol. The second pathway, leads to the formation of the anionic compound $C_3H_5O^-$ (m/z 57) and the loss off neutral molecule C_5H_8 (mass 68; see Fig. 4 below), with determined energy of 111 ($\pm$ 33) kJ/mol. Finally, a third observed fragmentation pathway gives a rise to the mass signal corresponding to the $C_4H_7^-$ (m/z 55) anion along with the formation of the neutral molecule C_4H_6O (mass 70). Extrapolation of the linearly rising section of the breakdown curve for m/z 55 gives an onset energy of 187 ($\pm$ 56) kJ/mol for this process.

### 3.2 Structural analysis of observed ion fragments

Further insight into the observed fragmentation pathway of deprotonated Norpinonic acid (*m/z* 169) was obtained through quantum chemical calculations. In particular, we applied three different Density Functional Theory (DFT) methods – ωB97XD/6-311+G(2d,p), CAM-B3LYP/6-311+G(2d,p) and PBE1PBE/6-311+G(2d,p) to explore the energetic and conformational landscape of observed fragmentation processes. In general, all employed methods were found to describe properly the main experimental observations. We have chosen to highlight in the main text the results obtained with the ωB97XD hybrid density functional since this method reproduces the experimental observation the most accurately (Chai and Head-Gordon, 2008). The computational method that most closely matched the experimental results was chosen on the basis of the correlation plots of the results. The correlation coefficient for the ωB97XD method was $R^2 = 0.76$ (Fig. 6) while that for the other two was 0.75 and 0.73 (PBE1PBE and B3LYP, respectively, Fig. S63, S64). For the comparison with the other theoretical results please consult the SI (Table S8-S10).

Reaction models for all observed fragmentation processes were computationally modeled, including determination of all possible transition states (TS) and alternative fragmentation pathways that forms the full reaction mechanism. The selection of the conformer od norpinonic acid goes according to the following procedure: the energies of all possible conformers are

175 optimized, and then statistical analysis is carried out according to the Boltzmann equation to select the conformer occurring in predominance. The potential energy surface for the first main fragmentation pathway that leads through the $C_8H_{13}O^-$ (*m/z* 125) anion formation to other smaller fragments, together with established chemical structures are shown in Fig. 4.
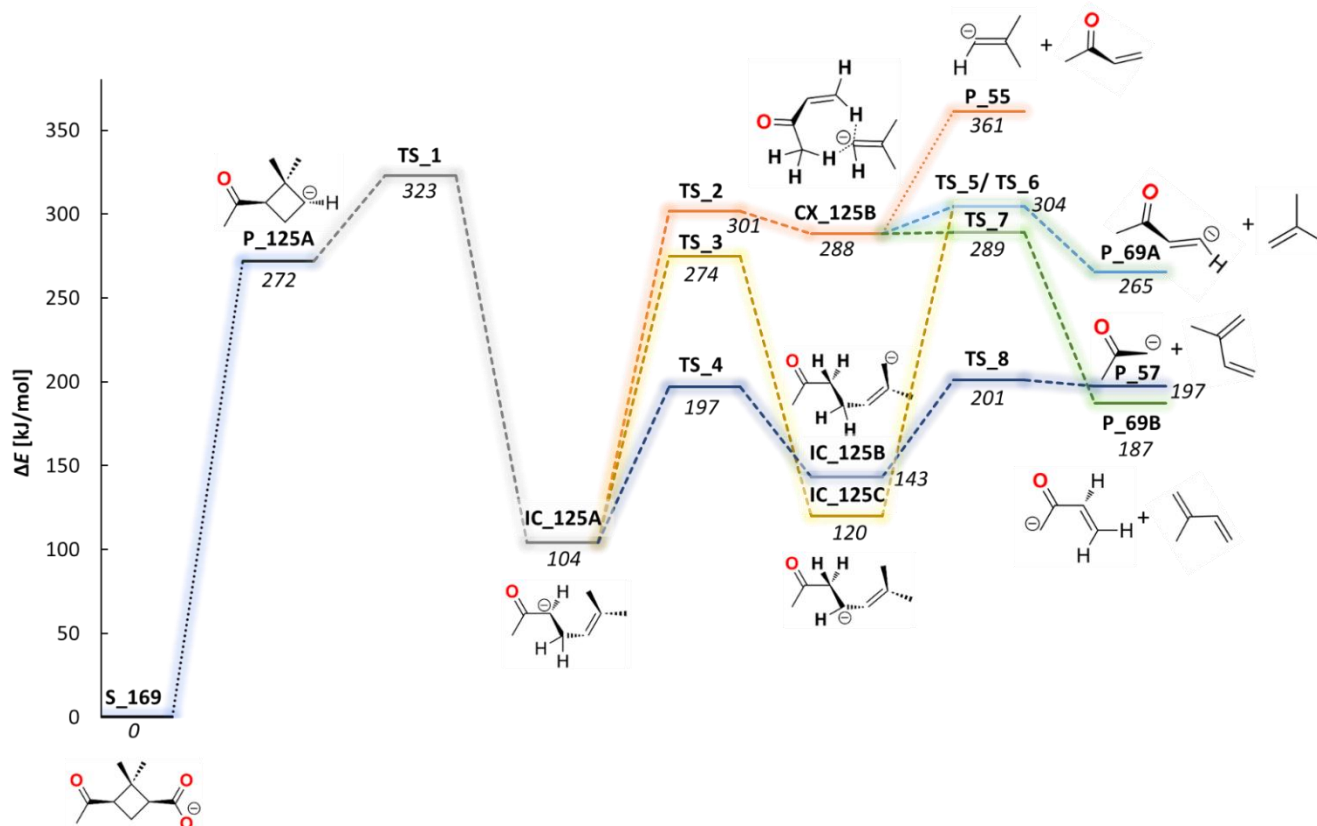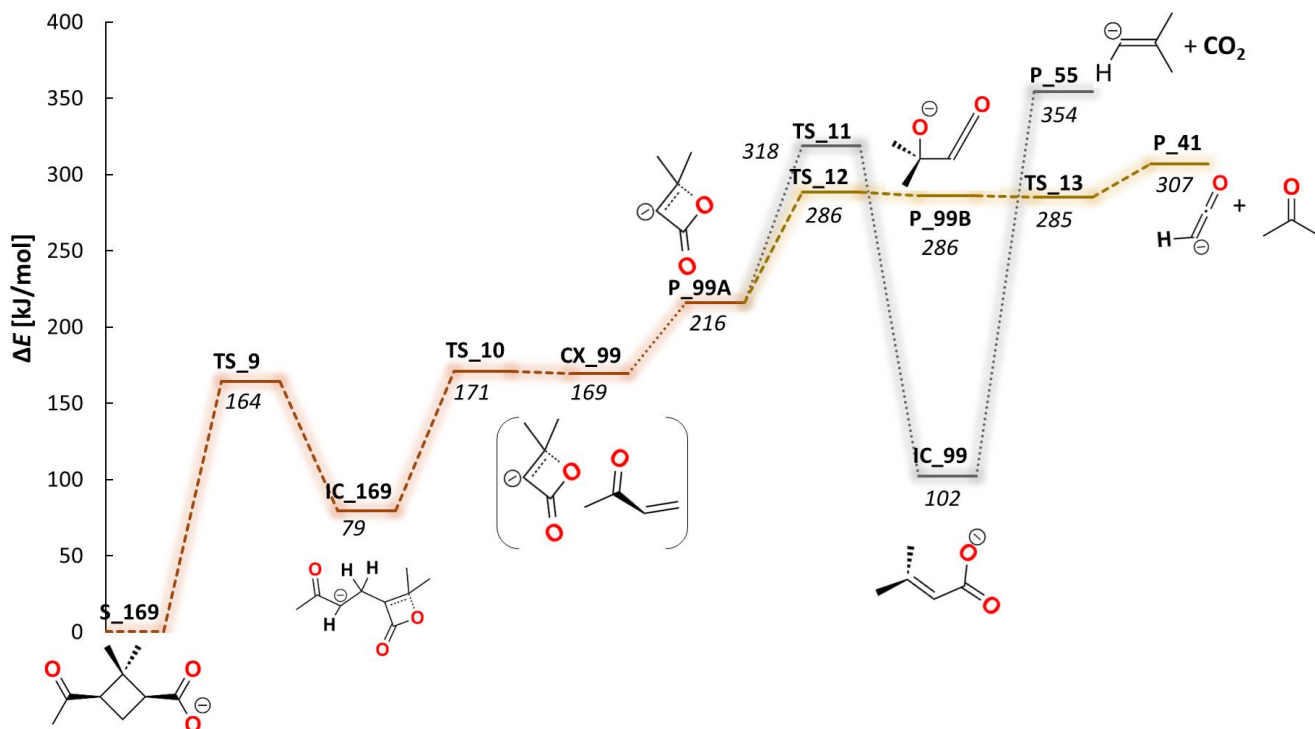

Figure 4. Computed potential energy (ωB97XD/6-311+G(2d,p)) diagrams describing first fragmentation pathway of m/z 169 ions
180 **via m/z 125 and further to smaller anionic fragments m/z 69, m/z 57, m/z 55. Abbreviations used in the structure names:**
S – Substrate, P – Product, TS – Transition State, IC– intermediate structure, and CX – intermediate complex.

Decarboxylation reaction of deprotonated Norpinonic acid $C_9H_{13}O_3^-$ (*m/z* 169) leads to the cyclic structure of *m/z* 125 (**P_125A**). Further DFT analysis of the fragmentation products anion *m/z* 125 has shown that **P_125A** is able to be rearranged by the cleavage of four-membered carbon ring to the more thermodynamically stable "open" structure **IC_125A** *via* relatively

185 low energy barrier **TS_1** at 51 kJ/mol above **P_125A** energy level. Interestingly, a similar breaking of a four-member ring had been formally reported earlier by Yasmeen et al, where the fragmentation of Norpinic acid − as a product of oxidation reaction of Norpinonic acid, has been discussed (Yasmeen et al., 2010). Notably, this observation has a fundamental impact on further mechanistic analysis and for understanding the thermodynamic and kinetic nature of generated ions. The m/z 125 ion is formed in the collision chamber of the mass spectrometer from the precursor ion m/z 169 (during ER-CID experiments). By precisely

190 dosing the ion collision energy, a kinetically controlled product (P_125A) is formed. Due to this fact an excellent correlation between the experimental (237 (± 70) kJ/mol) and computed energies (272 kJ/mol) for decarboxylation reaction of m/z 169

8

ion has been noted. On the other hand, to provide the quantitative energy measurements for subsequent fragmentations reactions of smaller fragments, the initial in-source fragmentation of m/z 169 was performed. Due to thermodynamic conditions of the electrospray ionization and fragmentation processes in the ion source, the in-source formed m/z 125 ions take more likely the "open" **IC_125A** isomeric form. Taking this into account, from this point the thermodynamic "open" isomer **IC_125A** start to play the reference role for subsequent measurements. In this respect, further collisional activation analysis of in-source formed m/z 125 ions has shown, that this anion undergoes three fragmentation pathways. Calculations of the first proposed fragmentation pathway of m/z 125 leads to m/z 55 anion *via* one transition state (**TS_2**) and intermediate structure **CX_125B**. It was found that anion $C_4H_7^-$ (m/z 55) is formed together with the neutral molecule C_4H_6O (mass 70), attributed to the methyl vinyl ketone (MVK) structure (**P°_70**), placed 257 kJ/mol above the **IC_125A** energy level. The **CX_125B** intermediate complex can also undergo alternative transformation through a transition state (**TS_5**) to anion m/z 69. Transition state energy (**TS_5**) was calculated to be 200 kJ/mol above **IC_125A** energy level. In this step of the reaction mechanism, the anion m/z 69 (**P_69A**) is formed, together with the neutral molecule C_4H_8 (mass 56), which corresponds to neutral molecule of 2-methylpropene chemical structure (**P°_56**). On the other hand, the alternative mechanism for m/z 69 anion formation may lead to **P_69B** structure through different transition state (**TS_7**), which has lower energetic requirements. The energy of **TS_7** was calculated at 185 kJ/mol above **IC_125A** energy level. Third calculated pathway leading to the formation of the anionic compound $C_3H_5O^-$ (m/z 57) by the loss of neutral fragment C_5H_8 (mass 68) corresponding to 2-metylobuta-1,3-dien structure, also known as isoprene (**P°_68**). It was found that two consecutive transition states leads to the formation of m/z 57 anion through IC_125B intermediate, calculated to be 197 kJ/mol and 201 kJ/mol, for **TS_4** and **TS_8**, respectively. Notably, the experimental appearance energy for m/z 57 formation estimated from the experiment (111 ($\pm$ 33) kJ/mol) is slightly higher than the computed transition state energy values (97 kJ/mol).

The second part of the potential energy diagram calculated for the fragmentation pathway of main m/z 169 anion that leads through m/z 99 ion to smaller ion fragments m/z 41 and 51 formation is shown in Fig. 5.

215 **Figure 5. Computed potential energy (ωB97XD/6-311+G(2d,p)) diagrams describing second fragmentation pathway of m/ z 169 ion via m/ z 99. Abbreviations used in the structure names: S – Substrate, P – Product, TS – Transition State, IC– intermediate structure, and CX – intermediate complex.**

It has been shown that the primary fragmentation product *m/z* 99 anion can form three alternative isomeric structures, a first where anion is located on the carbon atom (**P_99A**) or second, where negative charge occurs on oxygen atom (**P_99B**) and

220 intermediate product (**IC_99**). Structure **P_99A** is formed in exothermic process, that formally proceeds through two transition states − **TS_9** and **TS_10** and two intermediate mechanistic point, intermediate structure **IC_169** and complex **CX_99** with the ultimate reaction energy for **P_99A** calculated at 216 kJ/mol. This part of the mechanism can be referred to the kinetic ER-CID experimental results with estimated energy for *m/z* 99 ion formation at 245 kJ/mol. Based on the computed chemical transformations of the m/z 99 ion it is seen that the more thermodynamically stable isomer **P_99B** can be formed *via* opening

225 of lactone ring that is emphasized by the transition state **TS_12**, located 70 kJ/mol above **P_99A** energy level. It is worth mentioning, that further separate ER-CID experiments performed on *m/z* 99 anion, required it's initial in-source generation. In this respect, we think that again here, the more thermodynamically stable isomer of m/z 99 anion **P_99A** is formed while generated in the ion source, from which further experimental measurements in the collision cell took place.

The DFT computations show that after transition state **TS_12**, the isomer **P_99B** is formed, from which a exothermic path

230 lead to the formation of anion *m/z* 41 by the loss of neutral molecule C_3H_6O. Fragmentation reaction mechanism has shown that anion *m/z* 41 refers to ketene anion structure. Notably, the experimental appearance energies for *m/z* 41 formation reaction estimated from experiments (72 (± 22) kJ/mol) and the computed energy values as an energy difference between **P_99A** and

P_41 (91 kJ/mol) show very good correlation. The anion m/ z 55 is generated by decarboxylation reaction of anion m/z 99 (**IC_99**). The energy calculated for this process was found to be 252 kJ/mol. Calculated energy of anion *m/z* 55 formation reaction is slightly higher than experimental energy estimated with the extrapolation procedure which has been determined as 189 kJ/mol (Fig. 6, Table 1.).
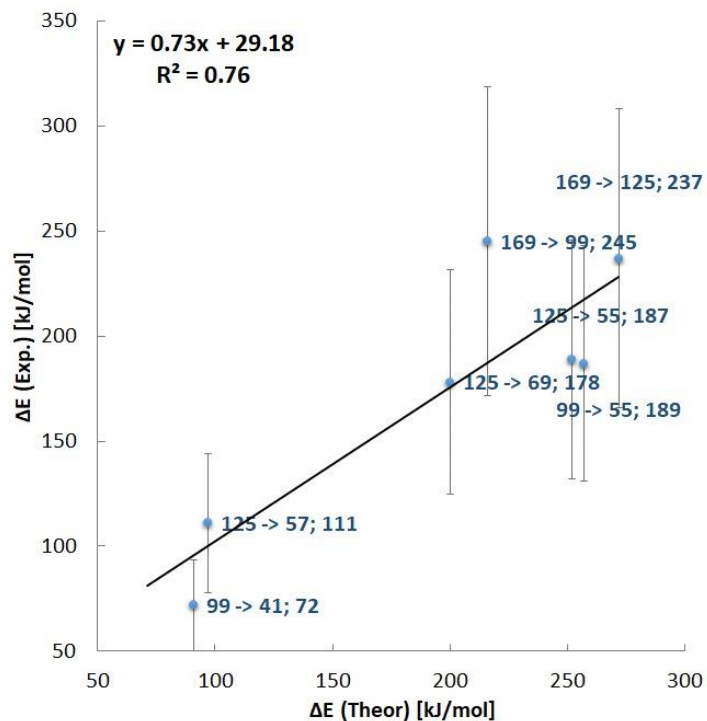

Figure 6. A correlation between experimental and theoretical fragmentation energies obtained with ωB97XD/6-311+G(2d,p) level of theory.

Table 1. Calculated electron energy values and experimental values in kJ/mol for fragmentation reaction of m/z 169 anion.

	Ion masses	Experimental Energy (kJ/mol)	Structure symbols	Theoretical method wB97XD/6-311+G(2d,p) (kJ/mol)
Fragmentation reaction	169 → 99	245 (± 73)	S_169 → P_99A	216
	99 → 55	189 (± 57)	IC_99 → P_55	252
	99 → 41	72 (± 22)	P_99A→ P_41	91
	169 → 125	237 (± 70)	S_169→P_125A	272
	125 → 69	178 (± 53)	IC_125A→TS_5	200
	125 → 57	111 (± 33)	IC_125A→TS_8	97
	125 → 55	187 (± 56)	IC_125A→P_55	257

11

The experimental and the theoretical insight into the fragmentation of deprotonated Norpinonic acid *m/z* 169 show, that fragmentation through a four-member ring breaking, leading to *m/z* 99 is a more energetically favorable process than decarboxylation reaction. It was also reported than anion *m/z* 99 form two possible structures, which differ in the location of

245   the negative charge (**P_99A** and **P_99B**), see Fig. 4. Furthermore, from quantum chemical calculations, the existence of two possible structure were found also for anion *m/z* 69 (**P_69A** and **P_69B**) as well as, for anion *m/z* 125 (**P_125A** and **P_125B**), see Fig 4.

3.3 Proton Affinity analysis of anionic fragments

In order to provide more arguments and confirm ion structures formed during ER-CID experiments, we decided to examine
250   the proton-transfer reactivity of all formed fragments towards few different proton-donors as neutral reagents, i.e. methyl thiocyanate (CH_3SCN), dimethyl disulfide (CH_3SSCH_3), chloroform ($CHCl_3$), bromoform ($CHBr_3$), dichloromethane (CH_2Cl_2) and nitromethane (CH_3NO_2). The above chemicals have been chosen as a natural representation of species being present in the atmosphere, while their anions provides a wide range of Proton Affinity (PA) values that gives a chance to investigate a proton transfer reaction with Norpinonic acid fragmentation products (Jia et al., 2018; Hossaini et al., 2017;
255   Watts, 2000; Graedel, 2012; Khalil and Rasmussen, 1999; Van Den Berg et al., 1994; Van Den Berg, 1993). The following Norpinonic acid anionic fragments were isolated as a result of the in-source generation/fragmentation and subjected into collision cell to perform a bimolecular reaction with neutral species: $C_9H_{13}O_3^-$ (*m/z* 169), $C_8H_{13}O^-$ (*m/z* 125), $C_5H_7O_2^-$ (*m/z* 99), $C_3H_5O^-$ (*m/z* 57), $C_4H_5O^-$ (*m/z* 69), $C_4H_7^-$ (*m/z* 55) and C_2HO^- (*m/z* 41). Neutral reagents were introduced to the collision cell *via* an in-house built gas inlet system. For more details of the reaction conditions (vapor pressure of neutral reagents and
260   E_{CM}), please consult the SI (Figure S48-S61). The reactions in the gas phase between neutral reagents and generated anions have shown a number of a new products, which will be described and published in other work in near future. In this publication, the structural analysis of generated fragment anions will be performed based on the proton transfer reaction, which relies on differences between the proton affinities values of reacting ions and anionic forms of the vaporous neutral molecules. In Table 2 the results of the observed reactivity of fragment anions with a series of neutral reagents in proton transfer reaction is briefly
265   summarized.

Table 2. Proton transfer reaction observed with gas-phase reactions of generated anions with series of neutral reagents (✓ - reaction observed, − - reaction not observed).

A⁻	Proton transfer					
	CH_2Cl_2	$CHBr_3$	$CHCl_3$	CH_3NO_2	CH_3SCN	CH_3SSCH_3
m/z **169**	−	−	−	−	−	−
m/z **125**	−	✓	✓	✓	−	−
m/z **99**	−	✓	✓	✓	−	−
m/z **69**	✓	✓	✓	✓	✓	✓

m/z 57	–	✓	✓	✓	–	–
m/z 55	✓	✓	✓	✓	✓	✓
m/z 41	–	✓	✓	✓	–	–

Proton affinity for each possible fragmentation anion and for appropriate anions of the involved neutral reagents have been computed at ωB97XD/6-311+G(2d,p) level of theory are schematically presented in Fig. S65 in SI and Table 3. For exact proton affinity values calculated at CAM-B3LYP/6-311+G(2d,p) and PBE1PBE/6-311+G(2d,p) level of theory please see Supplementary Information. Proton affinities calculated for all fragment anions are within the range of 1378 kJ/mol for deprotonated Norpinonic acid (m/z 169) to 1709 kJ/mol for anion $C_4H_7^-$ (m/z 55). Computed structures of anion m/z 69 – **P_69A** and **P_69B** (see Fig. 4) have shown a significant difference in their proton affinity values. For anion **P_69A** proton affinity was calculated to be 1611 kJ/mol, while for structure **P_69B** – 1530 kJ/mol. The significant difference in proton affinity values was also found for two possible structures calculated for anion m/z 125. Proton affinity of structure **P_125A** was calculated at 1703 kJ/mol, while for structure **IC_125B** – 1539 kJ/mol. Proton affinity analysis has shown that structure **P_125A** is stronger base than structure **IC_125B**. Similar dependence has been also reported for structure **P_69A** and **P_69B**, where structure **P_69A** is a stronger base than structure **P_69B.** The proton affinity values computed for appropriate anions derived from neutral reagents proton affinities were found to be from 1468 kJ/mol for bromoform anion to 1570 kJ/mol for dichloromethane anion. Computed PA values for deprotonated neutral reagents were compared with experimental ones available in the literature and are in good agreement (Afeefy et al., 2011).

Table 3. Energy of Proton affinity of the anionic fragment structures, compared with energy of proton affinities of appropriate deprotonated reagents used in gas phase reactions obtained by theoretical calculation.

Substrates	Energy of Proton Affinity [kJ/mol]	Anion of neutral reactants	Energy of Proton Affinity [kJ/mol]
P_55	1709	$^-CHCl_2$	1570
P_125A	1703	$CH_3SSCH_2^-$	1550
P_69A	1611	CH_2SCN^-	1549
P_99A	1560	$^-CCl_3$	1501
P_57	1540	$^-CH_2NO_2$	1478
IC_125	1539	$^-CBr_3$	1468
P_69B	1530		
P_41	1527		
P_99B	1434		
S_169	1378		

The proton transfer reaction with all neutral reagents was observed only for anions m/z 69 and m/z 55. Dichloromethane was found to react rapidly with anion m/z 55 in proton transfer reaction. Similar results were obtained in reaction with methyl thiocyanate as well as, with dimethyl disulfide. The relative intensity of the products for both reagents was low – 2.0 % for

anion *m/z* 55 and 0.1 % for anion *m/z* 69 (dimethyl disulfide reaction), 1.8 % for anion *m/z* 55 and 0.1 % for anion *m/z* 69

290   (methyl thiocyanate reaction). In the reaction of generated fragments with chloroform, bromoform as well as nitromethane we obtained similar/comparable results. The proton transfer reaction was observed for all studied fragments, except anion *m/z* 169. Anions *m/z* 125, *m/z* 69, *m/z* 57 and *m/z* 55 were found to react rapidly with chloroform, the products of proton transfer reaction were the most abundant. For reaction towards nitromethane, high intensity of proton transfer reaction product was observed for anions *m/z* 55 and *m/z* 57. Mass spectra of the reaction of chloroform, bromoform, dichloromethane and

295   nitromethane towards anion $C_9H_{13}O_3^-$ (*m/z* 169), $C_8H_{13}O^-$ (*m/z* 125), $C_5H_7O_2^-$ (*m/z* 99), $C_3H_5O^-$ (*m/z* 57), $C_4H_5O^-$ (*m/z* 69), $C_4H_7^-$ (*m/z* 55) and C_2HO^- (*m/z* 41) together with a relative intensity of proton transfer reaction product are presented in Fig. 7. For mass spectra of the reaction with methyl thiocyanate as well as, with dimethyl disulfide please consult Supplementary Information (Figure S48-S61).
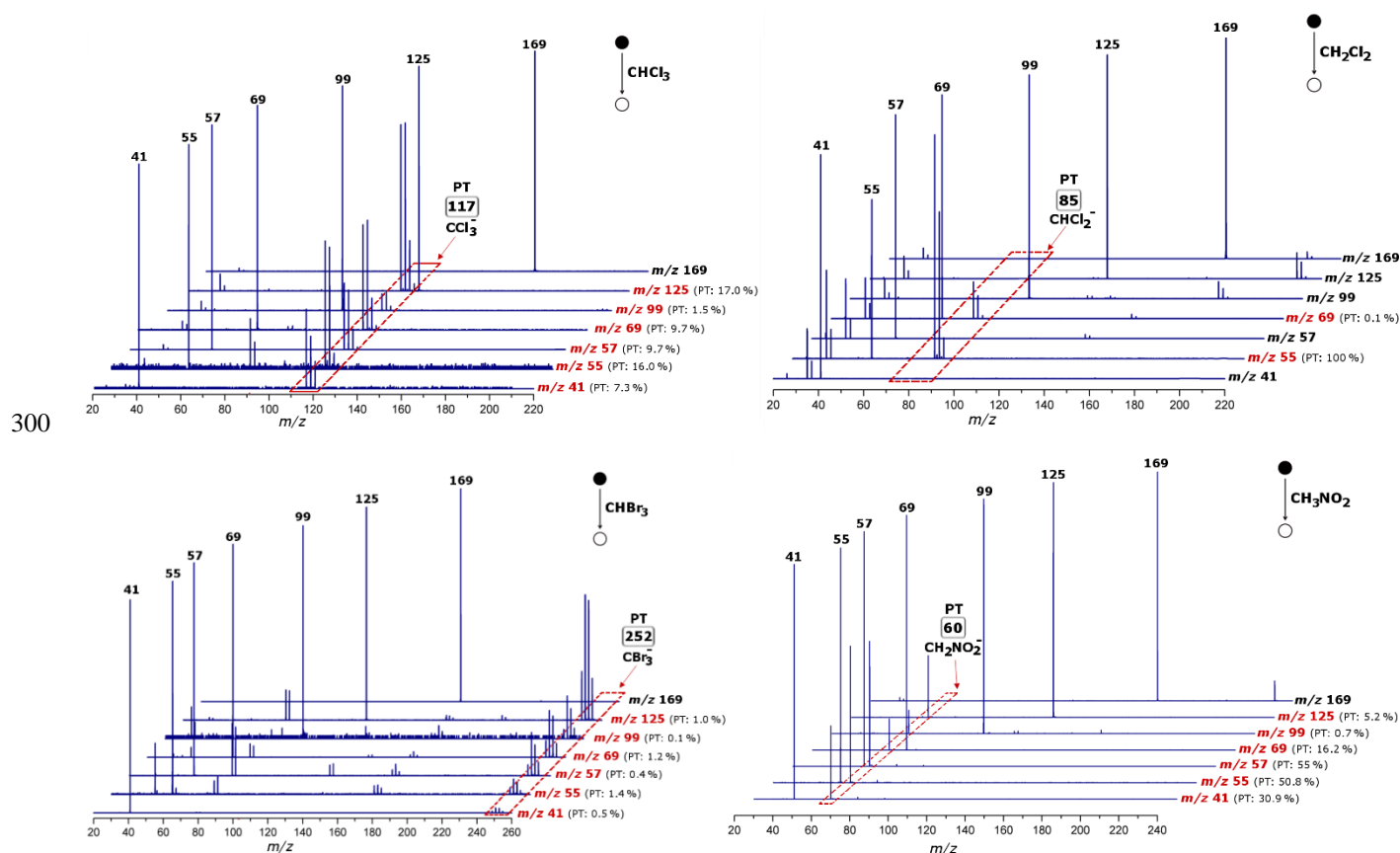
300

Figure 7. Mass spectra of the reactions between the neutral reagents (chloroform, bromoform, dichloromethane and nitromethane) and the ion source generated fragments recorded with a ToF voltage of 3kV, taken with reagents vapors at nominal pressures 3.25×10^{-4} mBar, 2.5×10^{-4} mBar, 3.05×10^{-4} mBar 3.14×10^{-4} mBar, respectively. For the collision energy (ECM) for each anion please

305   **consult the Supplementary Information.**

14

Quantum chemical calculations and gas – phase reactions together with proton affinity analysis turned out to be important to distinguished the structures formed during the collision-induced dissociation (CID) experiments. Quantum chemical calculations have shown two possible structures of anion m/z 125. However, an analysis of secondary fragmentation products of anion m/z 125 together with analysis of threshold energies, have shown that **P_125A** is able to rearrange to the more stable structure **IC_125A**. It appears rational that anion **P_125A** is formed in the collision cell during CID experiments of the precursor ion m/z 169 – experimental and theoretical threshold energies shown good correlation, while in the ion source, generated anion can rearrange to the more stable linear structure **IC_125A**. Furthermore, in the gas-phase reaction between anion m/z 125 and dichloromethane, methyl thiocyanate as well as, dimethyl disulfide proton transfer reaction products were not observed. This argument also confirms the hypothesis of the two possible structure of anion m/z 125, since proton affinity value for **P_125A** was calculated to be 1703 kJ/mol (proton transfer reaction product expected), since for structure **IC_125A** 1558 kJ/mol (value lower that proton affinity of dichloromethane, methyl thiocyanate and dimethyl disulfide – a proton transfer reaction should not occur and was not observed). Two possible structures have been also computed for anion m/z 69. It was found that anion **P_69B** need slightly lower energetic requirements to be formed, than anion **P_69A**, but the difference is not significant to unambiguously indicate the structure **P_69B** as the one. For anion m/z 69 a small amount of product of proton transfer reaction was observed in reaction with all neutral reagents, which clearly proves the presence of **P_69A** during ER-CID experiments. However, the combination of the lower energetic requirements obtained from quantum chemical computation for anion **P_69B** together with a higher proton affinity for **P_69A** has shown that both structures are possible to be generated in ER-CID experiments. In accordance with the computational model anion m/z 99 can form two possible structures, a first, where anion is located on the carbon atom (**P_99A**) or second, where anion is localized on oxygen atom (**P_99B**). Calculated PA value for structure **P_99A** is 1557 kJ/mol, while for **P_99B** 1449 kJ/mol. The gas-phase reactions of the m/z 99 anion with chloroform, bromoform and nitromethane give rise to a detectable amount of proton transfer reaction products, which clearly indicates the presence of at least some of **P_99A** structures during ER-CID experiments.

4 Conclusion

The study of the fragmentation pathways of deprotonated Norpinonic acid (important α-pinene oxidation product) was conducted together with structural analysis of the fragments generated during the energy resolved collision-induced dissociation (ER-CID) experiments. We have shown that quantum chemical calculations and gas-phase reactions supported by proton affinity analysis are reliable methods for the structural analysis of the deprotonated Norpinonic acid (m/z 169) fragments.

The breakdown curves for all fragment ions were also measured at variable collision energies and at five different collision gas pressures to estimate the threshold energies, which were measured to be from 72 kJ/mol for m/z 41 formation reaction to 245 kJ/mol for ion m/z 99 formation. Further insight into the observed fragmentation pathway of deprotonated Norpinonic acid was obtained through quantum chemical calculations. Comparison between the experimental and the theoretical threshold

energies calculated with ωB97XD/6-311+G(2d,p) level of theory has shown a good correlation - coefficient of determination (R^2) was found to be 0.76. Reaction models for observed fragmentation processes were constructed. Also the minimum energy
340 pathway (MEP) are investigated and presented

Finally, to distinguished all possible ion structures generated during ER-CID experiments, we examined the reactivity of all fragments towards a series of different neutral reagents - methyl thiocyanate (CH_3SCN), dimethyl disulfide (CH_3SSCH_3), chloroform ($CHCl_3$), bromoform ($CHBr_3$), dichloromethane (CH_2Cl_2) and nitromethane (CH_3NO_2). For structural analysis of generated anions, products of the gas - phase reactions were analyzed for proton transfer reaction. It was found that anions m/z
345 125, m/z 99 and m/z 69 can formed two possible structures.

Quantum chemical calculations and the gas-phase reactions together with proton affinity analysis turned out to be an valuable method to reflect the proper structures formed during energy-resolved collision-induced dissociation (ER-CID) experiments. Fragmentation structure proposed for an important α-pinene aging product (Norpinonic acid), serve as a useful databank for the atmospheric community and is believed to be extended in the future, towards other important aerosol products, including
350 different monoterpene SOA.

Author Contributions

IK performed a part of DFT computations and co-write the manuscript, AB performed the experiments and DFT computations, KP analyzed a part of experimental breakdown curves, KK co-write the manuscript, co-write the manuscript, KB coordinated the project, experiments and theoretical computations, co-write the manuscript. All authors have given approval to the final
355 version of the manuscript.

Competing interests

The authors declare no competing financial interest.

16

References

Afeefy, H., Liebman, J., and Stein, S.: NIST Chemistry WebBook, NIST Standard Reference Database Number 69, Linstrom PJ, Mallard WG, editors, 2011.

370 Blanco-Heras, G. A., Turnes-Carou, M. I., López-Mahía, P., Muniategui-Lorenzo, S., Prada-Rodríguez, D., and Fernández-Fernández, E.: Determination of organic anions in atmospheric aerosol samples by capillary electrophoresis after reversed pre-electrophoresis, Electrophoresis, 29, 1347-1354, 10.1002/elps.200700413, 2008.

Blaziak, K., Tzeli, D., Xantheas, S. S., and Uggerud, E.: The activation of carbon dioxide by first row transition metals (Sc–Zn), Phys. Chem. Chem. Phys., 20, 25495-25505, 10.1039/C8CP04231D, 2018.

375 Błaziak, K., Miller, G. B. S., Ryding, M. J., and Uggerud, E.: Reaction Model for the Formation of Benzene from Benzoates and Grignard Reagents, Eur. J. Org. Chem., 2017, 4272-4276, 10.1002/ejoc.201700816, 2017.

Chai, J.-D. and Head-Gordon, M.: Long-range corrected hybrid density functionals with damped atom–atom dispersion corrections, Phys. Chem. Chem. Phys., 10, 6615-6620, 10.1039/B810189B, 2008.

Christoffersen, T. S., Hjorth, J., Horie, O., Jensen, N. R., Kotzias, D., Molander, L. L., Neeb, P., Ruppert, L., Winterhalter, R.,
380 Virkkula, A., Wirtz, K., and Larsen, B. R.: cis-pinic acid, a possible precursor for organic aerosol formation from ozonolysis of α-pinene, Atmos. Environ., 32, 1657-1661, https://doi.org/10.1016/S1352-2310(97)00448-2, 1998.

Claeys, M., Szmigielski, R., Kourtchev, I., Van der Veken, P., Vermeylen, R., Maenhaut, W., Jaoui, M., Kleindienst, T. E., Lewandowski, M., Offenberg, J. H., and Edney, E. O.: Hydroxydicarboxylic Acids: Markers for Secondary Organic Aerosol from the Photooxidation of α-Pinene, Environ. Sci. Technol., 41, 1628-1634, 10.1021/es0620181, 2007.

385 Claeys, M., Iinuma, Y., Szmigielski, R., Surratt, J. D., Blockhuys, F., Van Alsenoy, C., Böge, O., Sierau, B., Gómez-González, Y., Vermeylen, R., Van der Veken, P., Shahgholi, M., Chan, A. W. H., Herrmann, H., Seinfeld, J. H., and Maenhaut, W.: Terpenylic Acid and Related Compounds from the Oxidation of α-Pinene: Implications for New Particle Formation and Growth above Forests, Environ. Sci. Technol., 43, 6976-6982, 10.1021/es9007596, 2009.

Dennington R., K. T., Millam J.: GaussView, Version 5.0.8 [dataset], 2009.

390 E. Jenkin, M., Shallcross, D. E., and Harvey, J. N.: Development and application of a possible mechanism for the generation of cis-pinic acid from the ozonolysis of α- and β-pinene, Atmos. Environ., 34, 2837-2850, https://doi.org/10.1016/S1352-2310(00)00087-X, 2000.

Feltracco, M., Barbaro, E., Contini, D., Zangrando, R., Toscano, G., Battistel, D., Barbante, C., and Gambaro, A.: Photo-oxidation products of α-pinene in coarse, fine and ultrafine aerosol: A new high sensitive HPLC-MS/MS method, Atmos.
395 Environ., 180, 149-155, https://doi.org/10.1016/j.atmosenv.2018.02.052, 2018.

Finessi, E., Decesari, S., Paglione, M., Giulianelli, L., Carbone, C., Gilardoni, S., Fuzzi, S., Saarikoski, S., Raatikainen, T., Hillamo, R., Allan, J., Mentel, T. F., Tiitta, P., Laaksonen, A., Petäjä, T., Kulmala, M., Worsnop, D. R., and Facchini, M. C.: Determination of the biogenic secondary organic aerosol fraction in the boreal forest by NMR spectroscopy, Atmos. Chem. Phys., 12, 941-959, 10.5194/acp-12-941-2012, 2012.

400 George, I. J. and Abbatt, J. P. D.: Chemical evolution of secondary organic aerosol from OH-initiated heterogeneous oxidation, Atmos. Chem. Phys., 10, 5551-5563, 10.5194/acp-10-5551-2010, 2010.

Glasius, M., Lahaniati, M., Calogirou, A., Di Bella, D., Jensen, N. R., Hjorth, J., Kotzias, D., and Larsen, B. R.: Carboxylic Acids in Secondary Aerosols from Oxidation of Cyclic Monoterpenes by Ozone, Environ. Sci. Technol., 34, 1001-1010, 10.1021/es990445r, 2000.

405 Goldstein, A. H. G., I. E.: Known and Unexplored Organic Constituents in the Earth's Atmosphere, Environ. Sci. Technol., 41, 1514-1521, 10.1021/es072476p, 2007.

Gómez-González, Y., Wang, W., Vermeylen, R., Chi, X., Neirynck, J., Janssens, I. A., Maenhaut, W., and Claeys, M.: Chemical characterisation of atmospheric aerosols during a 2007 summer field campaign at Brasschaat, Belgium: sources and source processes of biogenic secondary organic aerosol, Atmos. Chem. Phys., 12, 125-138, 10.5194/acp-12-125-2012, 2012.

410 Graedel, T.: Chemical Compounds in The Atmosphere, Elsevier Science2012.

Hallquist, M., Wenger, J. C., Baltensperger, U., Rudich, Y., Simpson, D., Claeys, M., Dommen, J., Donahue, N. M., George, C., Goldstein, A. H., Hamilton, J. F., Herrmann, H., Hoffmann, T., Iinuma, Y., Jang, M., Jenkin, M. E., Jimenez, J. L., Kiendler-Scharr, A., Maenhaut, W., McFiggans, G., Mentel, T. F., Monod, A., Prévôt, A. S. H., Seinfeld, J. H., Surratt, J. D., Szmigielski, R., and Wildt, J.: The formation, properties and impact of secondary organic aerosol: current and emerging issues, Atmos. Chem. Phys., 9, 5155-5236, 10.5194/acp-9-5155-2009, 2009.

Hirsikko, A., Nieminen, T., Gagné, S., Lehtipalo, K., Manninen, H. E., Ehn, M., Hõrrak, U., Kerminen, V. M., Laakso, L., McMurry, P. H., Mirme, A., Mirme, S., Petäjä, T., Tammet, H., Vakkari, V., Vana, M., and Kulmala, M.: Atmospheric ions and nucleation: a review of observations, Atmos. Chem. Phys., 11, 767-798, 10.5194/acp-11-767-2011, 2011.

Hocart, C. H.: 9.10 - Mass Spectrometry: An Essential Tool for Trace Identification and Quantification, in: Comprehensive Natural Products II, edited by: Liu, H.-W., and Mander, L., Elsevier, Oxford, 327-388, https://doi.org/10.1016/B978-008045382-8.00187-8, 2010.

Hossaini, R., Chipperfield, M. P., Montzka, S. A., Leeson, A. A., Dhomse, S. S., and Pyle, J. A.: The increasing threat to stratospheric ozone from dichloromethane, Nature Communications, 8, 15962, 10.1038/ncomms15962 https://www.nature.com/articles/ncomms15962#supplementary-information, 2017.

International Union of, P. and Applied, C.: mass-to-charge ratio, in, 10.1351/goldbook.M03752,

Jarrold, C. C.: Probing Anion–Molecule Complexes of Atmospheric Relevance Using Anion Photoelectron Detachment Spectroscopy, ACS Physical Chemistry Au, 3, 17-29, 10.1021/acsphyschemau.2c00060, 2023.

Jia, Y., Tegtmeier, S., Atlas, E., and Quack, B.: How Marine Emissions of Bromoform Impact the Remote Atmosphere, Atmos. Chem. Phys. Discuss., 2018, 1-29, 10.5194/acp-2018-1194, 2018.

Kavouras, I. G., Mihalopoulos, N., and Stephanou, E. G.: Formation of atmospheric particles from organic acids produced by forests, Nature, 395, 683-686, 10.1038/27179, 1998.

Kavouras, I. G., Mihalopoulos, N., and Stephanou, E. G.: Secondary Organic Aerosol Formation vs Primary Organic Aerosol Emission: In Situ Evidence for the Chemical Coupling between Monoterpene Acidic Photooxidation Products and New Particle Formation over Forests, Environ. Sci. Technol., 33, 1028-1037, 10.1021/es9807035, 1999.

Khalil, M. A. K. and Rasmussen, R. A.: Atmospheric chloroform, Atmospheric Environment, 33, 1151-1158, https://doi.org/10.1016/S1352-2310(98)00233-7, 1999.

Kourtchev, I., Warnke, J., Maenhaut, W., Hoffmann, T., and Claeys, M.: Polar organic marker compounds in PM2.5 aerosol from a mixed forest site in western Germany, Chemosphere, 73, 1308-1314, https://doi.org/10.1016/j.chemosphere.2008.07.011, 2008.

Krivácsy, Z., Molnár, Á., Tarjányi, E., Gelencsér, A., Kiss, G., and Hlavay, J.: Investigation of inorganic ions and organic acids in atmospheric aerosol by capillary electrophoresis, Journal of Chromatography A, 781, 223-231, https://doi.org/10.1016/S0021-9673(97)00290-2, 1997.

Li, L., Dai, D., Deng, S., Feng, J., Zhao, M., Wu, J., Liu, L., Yang, X., Wu, S., Qi, H., Yang, G., Zhang, X., Wang, Y., and Zhang, Y.: Concentration, distribution and variation of polar organic aerosol tracers in Ya'an, a middle-sized city in western China, Atmospheric Research, 120-121, 29-42, https://doi.org/10.1016/j.atmosres.2012.07.024, 2013.

Lignell, H., Epstein, S. A., Marvin, M. R., Shemesh, D., Gerber, B., and Nizkorodov, S.: Experimental and Theoretical Study of Aqueous cis-Pinonic Acid Photolysis, J. Phys. Chem. A, 117, 12930-12945, 10.1021/jp4093018, 2013.

M. J. Frisch, G. W. T., H. B. Schlegel, G. E. Scuseria, M. A. Robb, J. R. Cheeseman, G. Scalmani, V. Barone, B. Mennucci, G. A. Petersson, H. Nakatsuji, M. Caricato, X. Li, H. P. Hratchian, A. F. Izmaylov, J. Bloino, G. Zheng, J. L. Sonnenberg, M. Hada, M. Ehara, K. Toyota, R. Fukuda, J. Hasegawa, M. Ishida, T. Nakajima, Y. Honda, O. Kitao, H. Nakai, T. Vreven, J. A. Montgomery, Jr., J. E. Peralta, F. Ogliaro, M. Bearpark, J. J. Heyd, E. Brothers, K. N. Kudin, V. N. Staroverov, R. Kobayashi, J. Normand, K. Raghavachari, A. Rendell, J. C. Burant, S. S. Iyengar, J. Tomasi, M. Cossi, N. Rega, J. M. Millam, M. Klene, J. E. Knox, J. B. Cross, V. Bakken, C. Adamo, J. Jaramillo, R. Gomperts, R. E. Stratmann, O. Yazyev, A. J. Austin, R. Cammi, C. Pomelli, J. W. Ochterski, R. L. Martin, K. Morokuma, V. G. Zakrzewski, G. A. Voth, P. Salvador, J. J. Dannenberg, S. Dapprich, A. D. Daniels, Ö. Farkas, J. B. Foresman, J. V. Ortiz, J. Cioslowski, and D. J. Fox: Gaussian [dataset], 2009.

Ma, Y., Russell, A. T., and Marston, G.: Mechanisms for the formation of secondary organic aerosol components from the gas-phase ozonolysis of α-pinene, Phys. Chem. Chem. Phys., 10, 4294-4312, 10.1039/B803283A, 2008.

Ma, Y., Luciani, T., Porter, R. A., Russell, A. T., Johnson, D., and Marston, G.: Organic acid formation in the gas-phase ozonolysis of α-pinene, Phys. Chem. Chem. Phys., 9, 5084-5087, 10.1039/B709880D, 2007.

460   McAlister, A. B., Vesto, J. I., Huang, A., Wright, K. A., McLaughlin Sta. Maria, E. J., Bailey, G. M., Kretekos, N. P., Baldwin, P. R., Carrasquillo, A. J., and LaLonde, R. L.: Reactivity of a Carene-Derived Hydroxynitrate in Mixed Organic/Aqueous Matrices: Applying Synthetic Chemistry to Product Identification and Mechanistic Implications, Atmosphere, 12, 1617, 2021.

McCrumb, J. L. and Arnold, F.: High-sensitivity detection of negative ions in the stratosphere, Nature, 294, 136-139, 10.1038/294136a0, 1981.

465   Miller, G. B. S., Esser, T. K., Knorke, H., Gewinner, S., Schöllkopf, W., Heine, N., Asmis, K. R., and Uggerud, E.: Spectroscopic Identification of a Bidentate Binding Motif in the Anionic Magnesium–CO2 Complex ([ClMgCO2]−), Angew. Chem., Int. Ed., 53, 14407-14410, 10.1002/anie.201409444, 2014.

Moglioni, A. G., García-Expósito, E., Aguado, G. P., Parella, T., Branchadell, V., Moltrasio, G. Y., and Ortuño, R. M.: Divergent Routes to Chiral Cyclobutane Synthons from (−)-α-Pinene and Their Use in the Stereoselective Synthesis of

470   Dehydro Amino Acids, The Journal of Organic Chemistry, 65, 3934-3940, 10.1021/jo991773c, 2000.

Nozière, B., Kalberer, M., Claeys, M., Allan, J., D'Anna, B., Decesari, S., Finessi, E., Glasius, M., Grgić, I., Hamilton, J. F., Hoffmann, T., Iinuma, Y., Jaoui, M., Kahnt, A., Kampf, C. J., Kourtchev, I., Maenhaut, W., Marsden, N., Saarikoski, S., Schnelle-Kreis, J., Surratt, J. D., Szidat, S., Szmigielski, R., and Wisthaler, A.: The Molecular Identification of Organic Compounds in the Atmosphere: State of the Art and Challenges, Chem. Rev. (Washington, DC, U. S.), 115, 3919-3983,

475   10.1021/cr5003485, 2015.

Olsson, P. Q. and Benner, R. L.: Atmospheric Chemistry and Physics: From Air Pollution to Climate Change By John H. Seinfeld (California Institute of Technology) and Spyros N. Pandis (Carnegie Mellon University). Wiley-VCH: New York. 1997. $89.95. xxvii + 1326 pp. ISBN 0-471-17815-2, J. Am. Chem. Soc., 121, 1423-1423, 10.1021/ja985605y, 1999.

Peeters, J., Vereecken, L., and Fantechi, G.: The detailed mechanism of the OH-initiated atmospheric oxidation of α-pinene:

480   a theoretical study, Phys. Chem. Chem. Phys., 3, 5489-5504, 10.1039/B106555F, 2001.

Resch, J., Wolfer, K., Barth, A., and Kalberer, M.: Effects of storage conditions on the molecular-level composition of organic aerosol particles, Atmos. Chem. Phys., 23, 9161-9171, 10.5194/acp-23-9161-2023, 2023.

Richards, D. S., Trobaugh, K. L., Hajek-Herrera, J., Price, C. L., Sheldon, C. S., Davies, J. F., and Davis, R. D.: Ion-molecule interactions enable unexpected phase transitions in organic-inorganic aerosol, Science Advances, 6, eabb5643,

485   doi:10.1126/sciadv.abb5643, 2020.

Rodriguez, A. A., Rafla, M. A., Welsh, H. G., Pennington, E. A., Casar, J. R., Hawkins, L. N., Jimenez, N. G., De Loera, A., Stewart, D. R., Rojas, A., Tran, M. K., Lin, P., Laskin, A., Formenti, P., Cazaunau, M., Pangui, E., Doussin, J. F., and De Haan, D. O.: Kinetics, Products, and Brown Carbon Formation by Aqueous-Phase Reactions of Glycolaldehyde with Atmospheric Amines and Ammonium Sulfate, Journal of Physical Chemistry A, 126, 5375-5385, 10.1021/acs.jpca.2c02606,

490   2022.

Ruff, D. J.: The Semi-Volatile Fraction of Atmospheric Aerosols, Thesis, Rochester Institute of Technology., 2018.

Sarang, K., Otto, T., Gagan, S., Rudzinski, K., Schaefer, T., Brüggemann, M., Grgić, I., Kubas, A., Herrmann, H., and Szmigielski, R.: Aqueous-phase photo-oxidation of selected green leaf volatiles initiated by OH radicals: Products and atmospheric implications, Science of The Total Environment, 879, 162622, https://doi.org/10.1016/j.scitotenv.2023.162622,

495   2023.

Seinfeld, J. H. and Pandis, S. N.: Atmospheric chemistry and physics: from air pollution to climate change, John Wiley & Sons2016.

Shao, Y., Voliotis, A., Du, M., Wang, Y., Pereira, K., Hamilton, J., Alfarra, M. R., and McFiggans, G.: Chemical composition of secondary organic aerosol particles formed from mixtures of anthropogenic and biogenic precursors, Atmospheric

500   Chemistry and Physics, 22, 9799-9826, 10.5194/acp-22-9799-2022, 2022.

Szmigielski, R., Surratt, J. D., Gómez-González, Y., Van der Veken, P., Kourtchev, I., Vermeylen, R., Blockhuys, F., Jaoui, M., Kleindienst, T. E., Lewandowski, M., Offenberg, J. H., Edney, E. O., Seinfeld, J. H., Maenhaut, W., and Claeys, M.: 3-methyl-1,2,3-butanetricarboxylic acid: An atmospheric tracer for terpene secondary organic aerosol, Geophys. Res. Lett., 34, https://doi.org/10.1029/2007GL031338, 2007.

505   Tajuelo, M., Rodriguez, A., Aranda, A., Díaz-de-Mera, Y., Tucceri, M. E., and Rodriguez, D.: Secondary organic aerosol formation from photooxidation of γ-butyro and γ-valero-lactone: A combined experimental and theoretical study, Atmospheric Environment, 276, 119051, https://doi.org/10.1016/j.atmosenv.2022.119051, 2022.

Takahama, S., Ruggeri, G., and Dillner, A. M.: Analysis of functional groups in atmospheric aerosols by infrared spectroscopy: sparse methods for statistical selection of relevant absorption bands, Atmos. Meas. Tech., 9, 3429-3454, 10.5194/amt-9-3429-2016, 2016.

510

van den Berg, F.: Measured and computed concentrations of methyl isothiocyanate in the air around fumigated fields, Atmospheric Environment. Part A. General Topics, 27, 63-71, https://doi.org/10.1016/0960-1686(93)90071-6, 1993.

Van Den Berg, F., Roos, A. H., Tuinstra, L. G. M. T., and Leistra, M.: Measured and computed concentrations of 1,3-dichloropropene and methyl isothiocyanate in air in a region with intensive use of soil fumigants, Water, Air, and Soil

515 Pollution, 78, 247-264, 10.1007/BF00483035, 1994.

Watts, S. F.: The mass budgets of carbonyl sulfide, dimethyl sulfide, carbon disulfide and hydrogen sulfide, Atmospheric Environment, 34, 761-779, https://doi.org/10.1016/S1352-2310(99)00342-8, 2000.

Winterhalter, R., Van Dingenen, R., Larsen, B. R., Jensen, N. R., and Hjorth, J.: LC-MS analysis of aerosol particles from the oxidation of α-pinene by ozone and OH-radicals, Atmos. Chem. Phys. Discuss., 2003, 1-39, 10.5194/acpd-3-1-2003,

520 2003.

Yasmeen, F., Vermeylen, R., Szmigielski, R., Iinuma, Y., Böge, O., Herrmann, H., Maenhaut, W., and Claeys, M.: Terpenylic acid and related compounds: precursors for dimers in secondary organic aerosol from the ozonolysis of α- and β-pinene, Atmos. Chem. Phys., 10, 9383-9392, 10.5194/acp-10-9383-2010, 2010.

Yu, Z., Jang, M., Zhang, T., Madhu, A., and Han, S.: Simulation of Monoterpene SOA Formation by Multiphase Reactions

525 Using Explicit Mechanisms, ACS Earth and Space Chemistry, 5, 1455-1467, 10.1021/acsearthspacechem.1c00056, 2021.

Zanca, N., Lambe, A. T., Massoli, P., Paglione, M., Croasdale, D. R., Parmar, Y., Tagliavini, E., Gilardoni, S., and Decesari, S.: Characterizing source fingerprints and ageing processes in laboratory-generated secondary organic aerosols using proton-nuclear magnetic resonance (1H-NMR) analysis and HPLC HULIS determination, Atmos. Chem. Phys., 17, 10405-10421, 10.5194/acp-17-10405-2017, 2017.

530 Zhang, X., McVay, R. C., Huang, D. D., Dalleska, N. F., Aumont, B., Flagan, R. C., & Seinfeld, J. H.: Formation and evolution of molecular products in α-pinene secondary organic aerosol., Proc. Natl. Acad. Sci. U. S. A., 112, 14168-14173, 2015.